Salgado, R., Lyamin, A. V., Sloan, S. W. & Yu, H. S. (2004). *Géotechnique* **54**, No. 5, 297–306

Two- and three-dimensional bearing capacity of foundations in clay

R. SALGADO,* A.V. LYAMIN,† S.W. SLOAN† and H. S. YU‡

Bearing capacity calculations are an important part of the design of foundations. Most of the terms in the bearing capacity equation, as it is used today in practice, are empirical. Shape factors for square and rectangular footings could not be derived in the past because three-dimensional bearing capacity computations could not be performed with any degree of accuracy. Likewise, depth factors could not be determined because rigorous analyses of foundations embedded in the ground were not available. In this paper, the bearing capacities of strip, square, circular and rectangular foundations in clay are determined rigorously based on finite element limit analysis. The results of the analyses are used to propose rigorous, definitive values of the shape and depth factors for foundations in clays. These results are helpful in reducing the uncertainties related to the method of analysis in bearing capacity calculations, paving the way for more cost-effective foundation design.

KEYWORDS: bearing capacity; design; numerical modelling and analysis; theoretical analysis; clays; limit state design/analysis

Les calculs de capacité porteuse sont une étape importante dans la conception des fondations. La plupart des termes de l'équation de capacité porteuse, telle qu'elle est utilisée aujourd'hui dans la pratique, sont empiriques. Dans le passé, les facteurs de forme pour les assises carrées et rectangulaires ne pouvaient pas être dérivés car on ne pouvait pas faire avec exactitude les calculs tridimensionnels de capacité porteuse. De même, les facteurs de profondeur ne pouvaient être déterminés car on ne disposait pas d'analyses rigoureuses pour les fondations enfouies dans le sol. Dans cet exposé, nous déterminons de manière rigoureuse les capacités porteuses de fondations longues, carrées, circulaires et rectangulaires dans de l'argile en nous basant sur des analyses limites d'éléments finis. Nous utilisons les résultats des analyses pour proposer des valeurs rigoureuses et définitives pour les facteurs de forme et de profondeur de fondations dans des argiles. Les résultats aident à réduire les incertitudes relatives à la méthode d'analyse dans les calculs de capacité porteuse, ce qui devrait permettre la conception de fondations plus économiques.

INTRODUCTION

Geotechnical engineers routinely use the bearing capacity equation (Terzaghi, 1943; Meyerhof, 1951, 1963; Brinch Hansen, 1970) to estimate the limit unit load, q_{bL} (referred to as the limit unit base resistance), that will cause a footing to undergo classical bearing capacity failure. For clays, the bearing capacity equation has the following form:

$$q_{bL,net} = q_{bL} - q_0 = s_c d_c N_c s_u \quad (1)$$

where N_c is a bearing capacity factor; s_u is a representative undrained shear strength; $q_0 = \gamma_m D$ is the surcharge at the footing base level; γ_m is the wet unit weight of soil; D is the distance from the ground surface to the base of the foundation element; s_c is a shape factor; and d_c is a depth factor.

The depth factor, d_c, is defined as the ratio of the net limit unit base resistance, $q_{bL} - q_0$, for a strip footing at depth D to that for an identical strip footing at the soil surface (for which $q_0 = 0$). The shape factor, s_c, is defined as the ratio of the limit unit base resistance of a footing of any shape bearing on the soil surface to that of a strip footing on the soil surface. The equation assumes implicitly that the shape and depth factors are independent. We shall examine this assumption later in the paper.

An exact theoretical solution for N_c was found in the early part of the twentieth century (Prandtl, 1920, 1921) by considering a strip footing resting on the surface of a material with shear strength s_u. In this case, $d_c = s_c = 1$ and $q_0 = 0$. An exact solution for a rigid circular footing resting on cohesive, frictionless (Tresca) soil was obtained by Eason & Shield (1960) using the slip-line method and invoking the Haar–Von Karman hypothesis to resolve the intermediate principal stress.

However, no exact solution for the bearing capacity of square or rectangular footings on the soil surface was ever found. Nor is an exact solution available for footings placed at some depth within the soil. Engineers have dealt with these problems by using values for both the shape and depth factors derived primarily from experimental observations. Based on a combination of these experimental results and approximate analyses (e.g. Meyerhof, 1951, 1963; Skempton, 1951), engineers were able to develop a foundation design framework that has been in place for many decades. However, uncertainties have always existed regarding the bearing capacity equation. Large safety factors have been used, in part to account for such uncertainties.

In this paper we present results of rigorous analyses that give definitive values of shape and depth factors for use in bearing capacity computations in clay. The correct shape and depth factors are determined by computing the bearing capacities of footings of various geometries placed at various depths and comparing those with the bearing capacities of strip footings located on the ground surface with the same soil conditions. All computations were performed for a rough soil–footing interface. The results presented in this paper lead, in effect, to the possibility of lower global safety factors for strip, square, circular or rectangular footings subjected to centred vertical loads. This is possible because the availability of a rigorous solution to the bearing capacity problem may justify a reduction of the component of the global safety factor attributable to analysis or 'model' uncertainty.

Manuscript received 24 December 2003; revised manuscript accepted 4 March 2004.
Discussion on this paper closes 1 January 2005, for further details see p. ii.
* School of Civil Engineering, Purdue University, USA.
† Department of Civil Engineering, University of Newcastle, NSW, Australia.
‡ School of Civil Engineering, University of Nottingham, UK.

REVIEW OF PREVIOUS WORK ON BEARING CAPACITY

It is conservative (but usually fairly realistic) to assume that foundations in clay are loaded under undrained conditions for typical foundation loading rates. The soil can be accordingly modelled as a material with $c = s_u$ and $\phi = 0$, where s_u is the undrained shear strength of the clay. For the case of a strip footing on the soil surface, equation (1) reduces to

$$q_{bL} = s_u N_c \tag{2}$$

where $N_c = 2 + \pi \approx 5{\cdot}14$ (an exact solution, first found by Prandtl 1920, 1921).

In order to compute the limit base resistance of square, circular or rectangular footings placed at different depths within the soil, correction factors (called shape and depth factors) are applied to equation (2), leading back to equation (1):

$$q_{bL} = s_c d_c N_c s_u + q_0$$

Shape factors allow conversion of values derived for strip footings to those appropriate for circular, square or rectangular footings. In clays, footings of finite plan dimension B and L have greater bearing capacity than strip footings with width B. The factor mostly responsible for this effect is the development of additional slip surfaces in front of and behind the footing. Depth factors, on the other hand, account for the fact that the slip surfaces do not develop only below the base of the footing, but also extend above the base of the footing to the surface of the soil. Table 1 contains the expressions more commonly used for these factors.

The equations in Table 1 are all empirical, as the theoretical basis for calculating collapse loads for footings under conditions other than plane strain was not previously available, and thus it could not be known by what factors to multiply $s_u N_c$ in order to obtain the bearing capacity of embedded circular, square or rectangular footings. The experimental data on which these equations are based are mostly due to Meyerhof (1951, 1963) and Skempton (1951), who tested both prototype and model foundations.

TWO- AND THREE-DIMENSIONAL FINITE-ELEMENT LIMIT ANALYSIS

Limit analysis: background

From the time Hill (1951) and Drucker *et al.* (1951, 1952) published their ground-breaking lower and upper bound theorems of plasticity theory, on which limit analysis is based, it was apparent that limit analysis was the tool that would lead to solutions of the bearing capacity problem and other stability problems. However, the numerical techniques required for finding very close lower and upper bounds on collapse loads, thus closely defining the collapse loads, were not available until very recently.

Limit analysis takes advantage of the lower and upper bound theorems of plasticity theory to bound the rigorous solution to a stability problem from below and above. The lower bound theorem states that collapse does not occur for a statically admissible stress field—a stress field that nowhere violates the yield criterion and is in equilibrium with the surface tractions and body forces. This can be written in the form of the virtual work equation as

$$\int_S T_i^L v_i \,\mathrm{d}S + \int_V X_i^L v_i \,\mathrm{d}V = \int_V \sigma_{ij}^L \dot{\varepsilon}_{ij} \,\mathrm{d}V \leqslant \int_V D(\dot{\varepsilon}_{ij}) \,\mathrm{d}V = \int_V \sigma_{ij} \dot{\varepsilon}_{ij} \,\mathrm{d}V \tag{3}$$

where σ_{ij}^L is a statically admissible stress field in equilibrium with the tractions T_i^L and the body forces X_i^L; σ_{ij} is the actual stress field; $\dot{\varepsilon}_{ij}$ is the actual strain rate field; and v_i is the actual velocity field. Note that, in the lower bound theorem, only the equilibrium equation, the yield criterion and the stress boundary conditions are considered. Kinematics is not taken into account.

The upper bound theorem states that collapse is either imminent or already under way for a kinematically admissible velocity field—a compatible velocity field that satisfies the flow rule and velocity boundary conditions. This can be written as follows:

$$\int_S T_i^U v_i^U \,\mathrm{d}S + \int_V X_i^U v_i^U \,\mathrm{d}V = \int_V \sigma_{ij}^U \dot{\varepsilon}_{ij}^U \,\mathrm{d}V = \int_V D(\dot{\varepsilon}_{ij}^U) \mathrm{d}V \geqslant \int_V \sigma_{ij} \dot{\varepsilon}_{ij}^U \,\mathrm{d}V \tag{4}$$

where $v_i^U$is a kinematically admissible velocity field compatible with the strain rate field $\dot{\varepsilon}_{ij}^U$; $\sigma_{ij}^U$is the stress field corresponding to the upper bound loading T_i^U and X_i^U; and σ_{ij} is the actual stress field. The upper bound theorem requires the flow rule, the compatibility condition and the velocity boundary conditions to be satisfied, but not the equilibrium equation.

In equations (3) and (4), the inequalities are due to the principle of maximum power dissipation. For the bearing capacity analysis of this paper, the collapse load is expressed in terms of the vertical load transmitted to the soil at the base of the footing.

Discrete formulation of lower bound theorem

As follows from the previous section, the objective of a lower bound calculation is to find a stress field σ_{ij} that satisfies equilibrium throughout the soil mass, balances the prescribed surface tractions, nowhere violates the yield criterion, and maximises the left side of equation (3). More simply, the stress field must maximise $\mathbf{Q}$, given by

$$\mathbf{Q} = \int_S \mathbf{T} \,\mathrm{d}S + \int_V \mathbf{X} \,\mathrm{d}V \tag{5}$$

In the present formulation of the lower bound theorem, linear finite elements are used to discretise the continuum, and statically admissible stress discontinuities are permitted at all interfaces between adjacent elements (Fig. 1(a)). If N is the problem dimensionality, then there are $N + 1$ nodes in each element, and each node is associated with a $(N^2 + N)/2$-dimensional vector of stress variables $\{\sigma_{ij}\}$, $i = 1 \ldots, N$; $j = 1, \ldots, N$. These stresses, together with the body force components X_i that act on a unit volume of material, are taken as the problem variables. The vector of unknowns for an element e is denoted by $\mathbf{X}^e$, and may be written as

Table 1. Shape and depth factors commonly used for clays

Shape factors	Depth factors	Author
$s_c = 1 + 0{\cdot}2B/L$	$d_c = 1 + 0{\cdot}2D/B$	Meyerhof (1951)
$s_c = 1 + 0{\cdot}2B/L$	$d_c = 1 + 0{\cdot}4D/B$ for $D/B < 1$ $d_c = 1 + 0{\cdot}4\tan^{-1}(D/B)$ for $D/B \geqslant 1$	Brinch Hansen (1970)

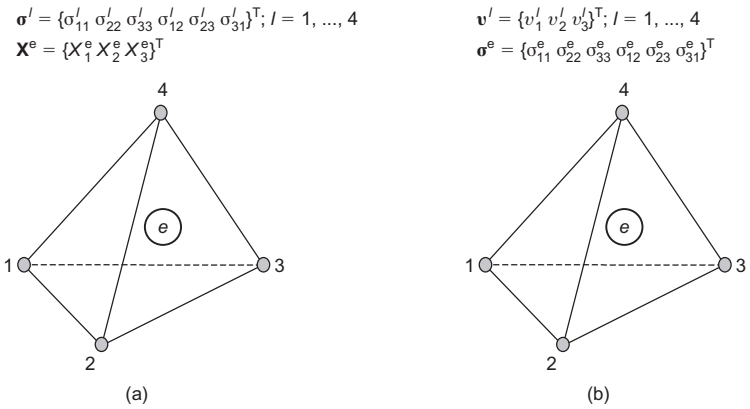

Fig. 1. Simplex finite elements for: (a) lower, and (b) upper bound limit analysis

$$\mathbf{x}^e = \left\{ \left\{\sigma^1_{ij}\right\}^T, \ldots, \left\{\sigma^{N+1}_{ij}\right\}^T, \left\{X^e_i\right\}^T \right\}^T;$$

$$i = 1, \ldots, N; \quad j = i, \ldots, N \tag{6}$$

In the context of mathematical optimisation, when the stress field is modelled using linear finite elements, the objective function and equality constraints arising from the equilibrium, boundary, discontinuity, and loading conditions are linear in the unknowns, with the only non-linearity arising from the yield inequalities. Thus the problem of finding a statically admissible stress field that maximises the collapse load may be stated as

$$\text{maximise} \quad \mathbf{c}^T\mathbf{x} \tag{7}$$

subject to

$$\mathbf{A}\mathbf{x} = \mathbf{b}$$
$$f_j(\mathbf{x}) \leqslant 0,$$
$$j \in J_x$$
$$\mathbf{x} \in \mathbb{R}^n$$

where $\mathbf{c}$ is an n-dimensional vector of objective function coefficients, $\mathbf{A}$ is an $m \times n$ matrix of equality constraint coefficients, $f_j(\mathbf{x})$ are yield and other inequality constraint functions, J_x is the set of inequality constraints on problem variables, $\mathbf{x}$ is an n-dimensional vector that is to be determined, and n is the number of unknown stresses and element unit weights.

A detailed description of a robust non-linear algorithm for solving the lower bound problem (equation (7)) can be found in Lyamin (1999) and Lyamin & Sloan (2002).

Discrete formulation of upper bound theorem

Referring to equation (4), the objective of an upper bound calculation is to find a velocity distribution, $\mathbf{v}$, that satisfies compatibility, the flow rule, and the velocity boundary conditions and, in addition, that minimises the internal power dissipation given by the integral

$$W^{\text{internal}} = \int_V \boldsymbol{\sigma}\dot{\boldsymbol{\varepsilon}}\, \mathrm{d}V \tag{8}$$

An upper bound estimate on the true collapse load can be obtained by equating W^{internal} to the power dissipated by the external loads:

$$W^{\text{external}} = \int_S \mathbf{T}^T\mathbf{v}\, \mathrm{d}S + \int_V \mathbf{X}^T\mathbf{v}\, \mathrm{d}V \tag{9}$$

The upper bound finite element used to discretise the continuum is shown in Fig. 1(b). Kinematically admissible velocity discontinuities are permitted at all interfaces between adjacent elements. Each node of the element is associated with an N-dimensional vector of velocity variables $\{v_i\}$, $i = 1, \ldots, N$. These, together with a $(N^2 + N)/2$-dimensional vector of elemental stresses $\{\sigma_{ij}\}$, $i = 1, \ldots, N$; $j = 1, \ldots, N$ and a $2(N - 1)$-dimensional vector of discontinuity variables, $\mathbf{w}$, are taken as the problem variables.

Applying the velocity boundary conditions, the flow rule constraints, and collecting terms for the power dissipated throughout the body, the problem of finding a kinematically admissible velocity field that minimises the internal power dissipation may be stated as

$$\text{minimise} \quad W = \boldsymbol{\sigma}^T\mathbf{B}\mathbf{v} + \mathbf{c}_v^T\mathbf{v} + \mathbf{c}_w^T\mathbf{w} \quad \text{on } (\mathbf{v}, \mathbf{w}) \tag{10}$$

subject to

$$\mathbf{A}_v\mathbf{v} + \mathbf{A}_w\mathbf{w} = \mathbf{b}$$
$$\mathbf{B}\mathbf{v} = \sum_{j \in J_\sigma} \lambda_j \nabla f_j(\boldsymbol{\sigma})$$
$$\lambda_j f_j(\boldsymbol{\sigma}) = 0, \quad j \in J_\sigma$$
$$f_j(\boldsymbol{\sigma}) \leqslant 0, \quad j \in J_\sigma$$
$$\lambda_j \geqslant 0, \quad j \in J_\sigma$$
$$\mathbf{w} \geqslant \mathbf{0}$$
$$\mathbf{v} \in {}^{n_v}, \quad \mathbf{w} \in \mathbb{R}^{n_w}, \boldsymbol{\sigma} \in \mathbb{R}^{n_\sigma}, \quad \boldsymbol{\lambda} \in \mathbb{R}^E$$

where $\mathbf{B}$ is an $n_\sigma \times n_v$ global compatibility matrix; $\mathbf{c}_v$ is an n_v-dimensional vector of objective function coefficients for the velocities; $\mathbf{c}_w$ is an n_w-dimensional vector of objective function coefficients for the discontinuity variables; $n_\sigma = EN(N + 1)$; $n_v = KN$ (K is the number of nodes and E is the number of elements in the mesh); $n_w = 2N(N - 1)D_s$; D_s is the total number of discontinuities; $\mathbf{A}_v$ is an $r \times n_v$ matrix of equality constraint coefficients for velocities; $\mathbf{A}_w$ is an $r \times n_w$ matrix of equality constraint coefficients for discontinuity variables; $r = N^2 D_s +$ number of boundary conditions and loading constraints; $f_j(\boldsymbol{\sigma})$ are yield functions, λ_j are non-negative multipliers; and $\mathbf{v}$, $\mathbf{w}$ and $\boldsymbol{\sigma}$ are problem unknowns.

A full description of a two stage, quasi-Newton strategy for solving the system (10) can be found in Lyamin & Sloan (2002a).

Typical meshes for embedded footing problem

In order to increase the accuracy of the computed depth factors for 3D problems for the same computation time, the symmetry inherent in all of these problems is fully

exploited. This means that only 15°, 45° and 90° sectors are discretised for the circular, square and rectangular footings. For strip footings, only half of the semi-space is discretised. These cases are shown in Figs 2–7. These plots also show the boundary conditions adopted in the various analyses and resultant plastic zones (shaded regions) and deformation patterns. The 15° sector for circular footings has been used to minimise computation time. The slice of such a thickness can be discretised using only one layer of well-shaped elements, while keeping the error in geometry representation below 1% (which is much less than the accuracy of the predicted collapse load).

For the lower bound meshes, special extension elements are included to extend the stress field over the semi-infinite domain (thus guaranteeing that the solutions obtained are rigorous lower bounds on the true solutions). To model the embedded conditions properly, the space above the footing has been filled with the soil mass, but at the same time preserving the gap between the top of the footing and this filling, which is supported by normal hydrostatic pressure, as shown in the enlarged diagrams of Figs 2 and 3. Rough conditions are applied at the top and bottom of the footing by prescribing zero tangential velocity for upper bound calculations and specifying no particular shear stresses for lower bound calculations (that is, the yield criterion is operative between the footing and the soil in the same way as it is operative within the soil).

LIMIT BEARING CAPACITY CALCULATIONS

Modelling of clay deposits

The theoretical profile of undrained shear strength, s_u, with depth for a uniform deposit of normally consolidated clay with groundwater table at the surface is linear, starting from zero at the ground surface, with s_u/σ'_v usually in the range 0·2–0·3. Values of s_u/σ'_v for overconsolidated clays take higher values, with the following equation commonly used to estimate them (Ladd *et al.*, 1977):

$$\frac{s_u}{\sigma'_v} = \left(\frac{s_u}{\sigma'_v}\right)_{NC} \mathrm{OCR}^{0·8} \tag{11}$$

In practice, clay deposits are often subject to some overconsolidation. It is not unusual to find deposits with an

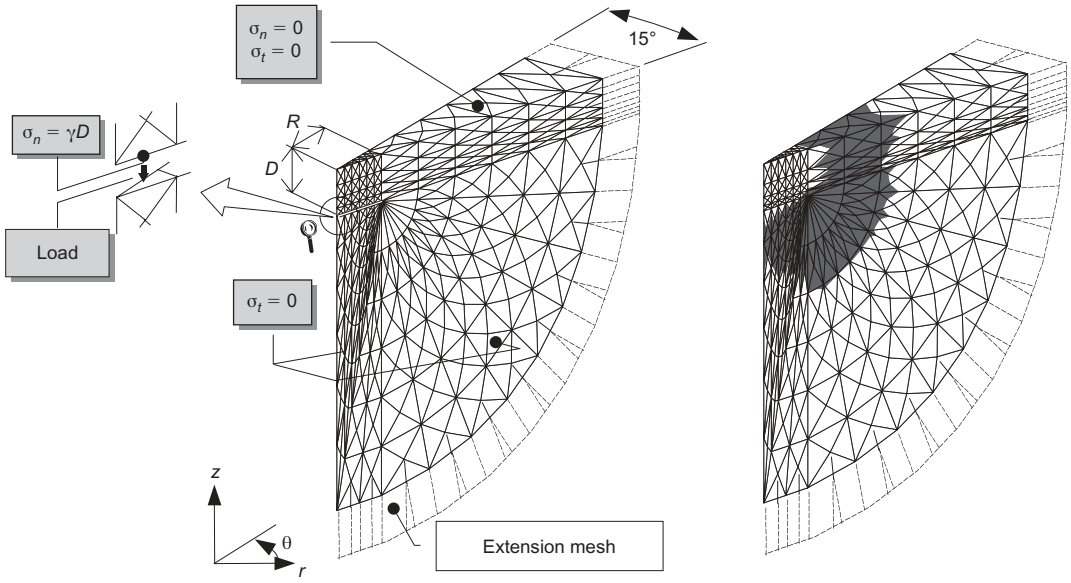

Fig. 2. Typical lower bound mesh and plasticity zones for circular footings

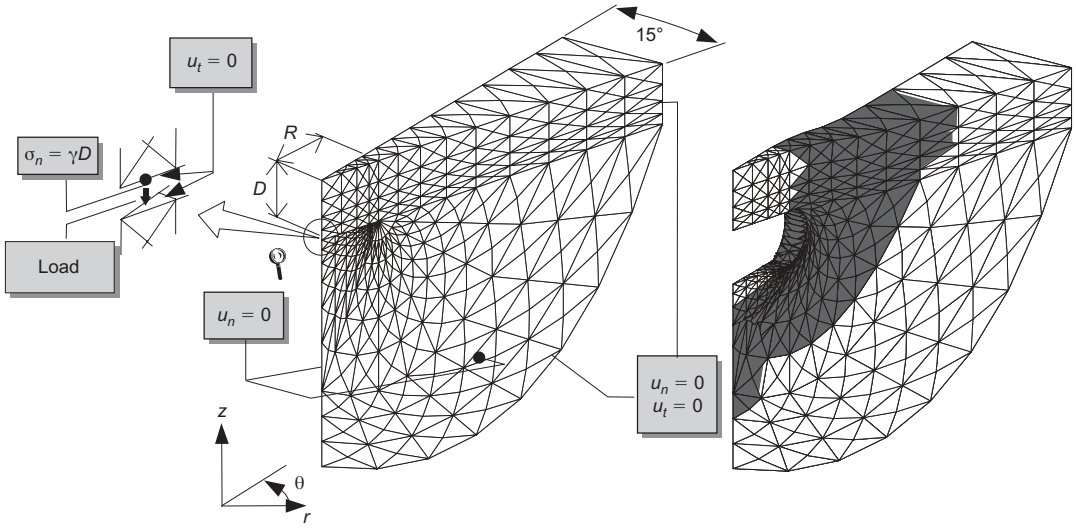

Fig. 3. Typical upper bound mesh and deformation pattern for circular footings

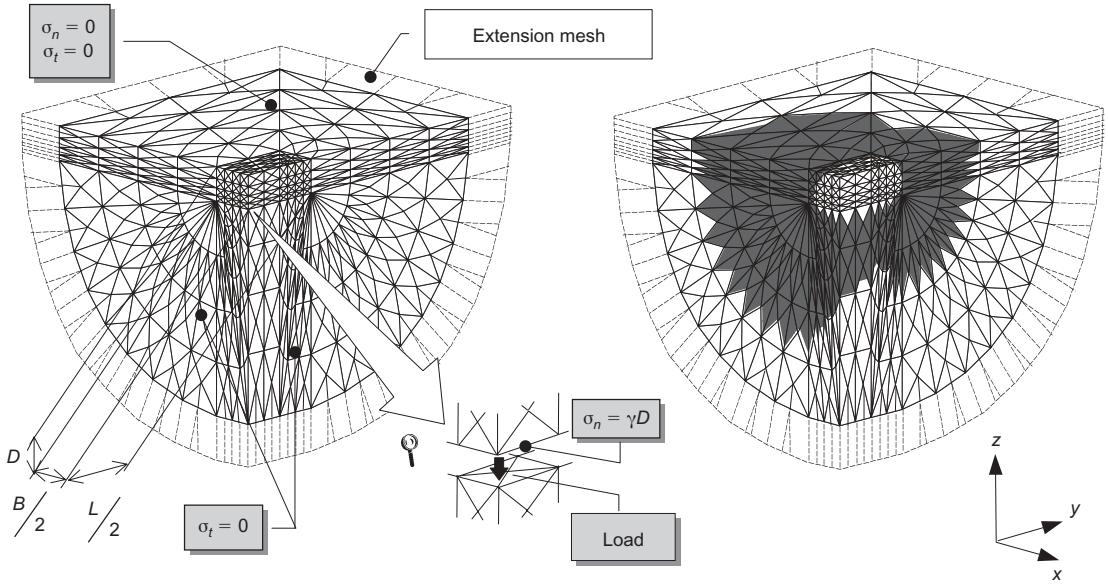

Fig. 4. Typical lower bound mesh and plasticity zones for rectangular footings

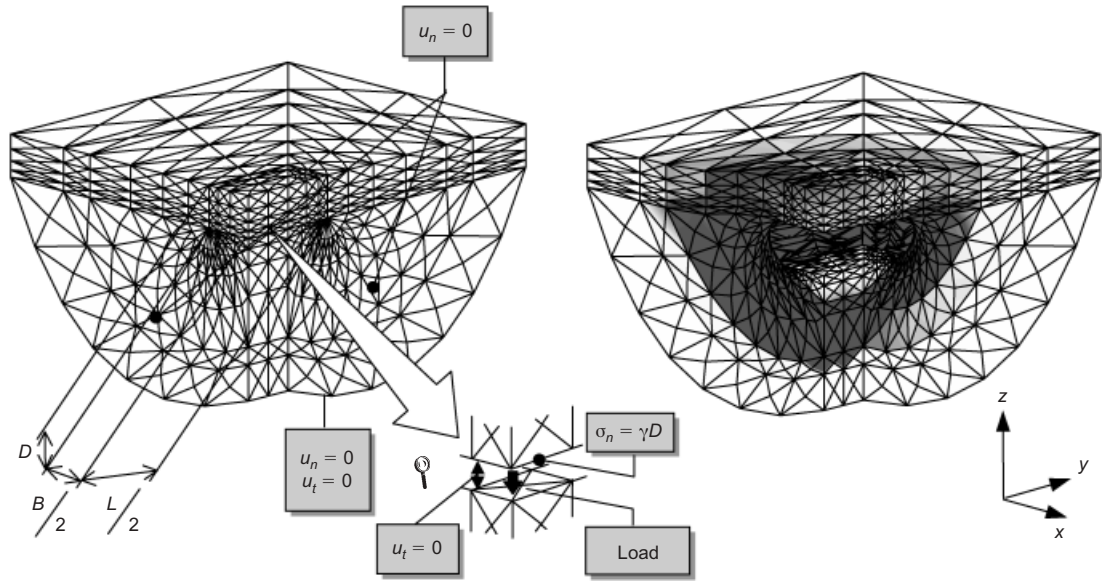

Fig. 5. Typical upper bound mesh and deformation pattern for rectangular footings

overconsolidated top layer, with OCR starting very high near the surface and dropping fast towards 1 as depth increases. The resulting s_u profile starts from a non-zero value at the surface and can often be assumed to be uniform with depth below the base of a footing placed within the overconsolidated layer, as the rising σ'_v partly compensates for the decreasing OCR (refer to equation (11)).

If overconsolidation is very superficial, the slip mechanism for the footing (which extends roughly B below the base of the footing, where B is the footing width) will reach into the normally consolidated soil. The slip mechanism for the footing then extends into the zone where s_u varies linearly with depth.

In calculations using the bearing capacity equation, it is common to work with a single, representative s_u value, with the implied assumption of a constant s_u with depth below the footing. Equation (11) suggests that this assumption is adequate for many overconsolidated soil deposits. For s_u profiles that vary with depth, an appropriate, representative value of s_u must be selected for use in the bearing capacity calculations. A simple way of doing this is to take an average of s_u values within a representative depth (roughly the depth to which the slip mechanism extends) below the footing base. For a deposit with uniform strength with depth, the representative depth is roughly equal to the footing width. For increasing strength with depth, Davis & Booker (1973) showed that the mechanism is shallower, and so should be the representative depth taken to estimate s_u. In all that we do next, a strength profile described by constant s_u with depth is assumed.

Strip foundations

Table 2 shows values of $q_{bL}^{net} = q_{bL} - q_0$ calculated for various foundation shapes and depths of embedment. Calculations performed both for $\gamma D/s_u = 1$ and for weightless soil confirm the numbers of Table 2, showing that the bearing

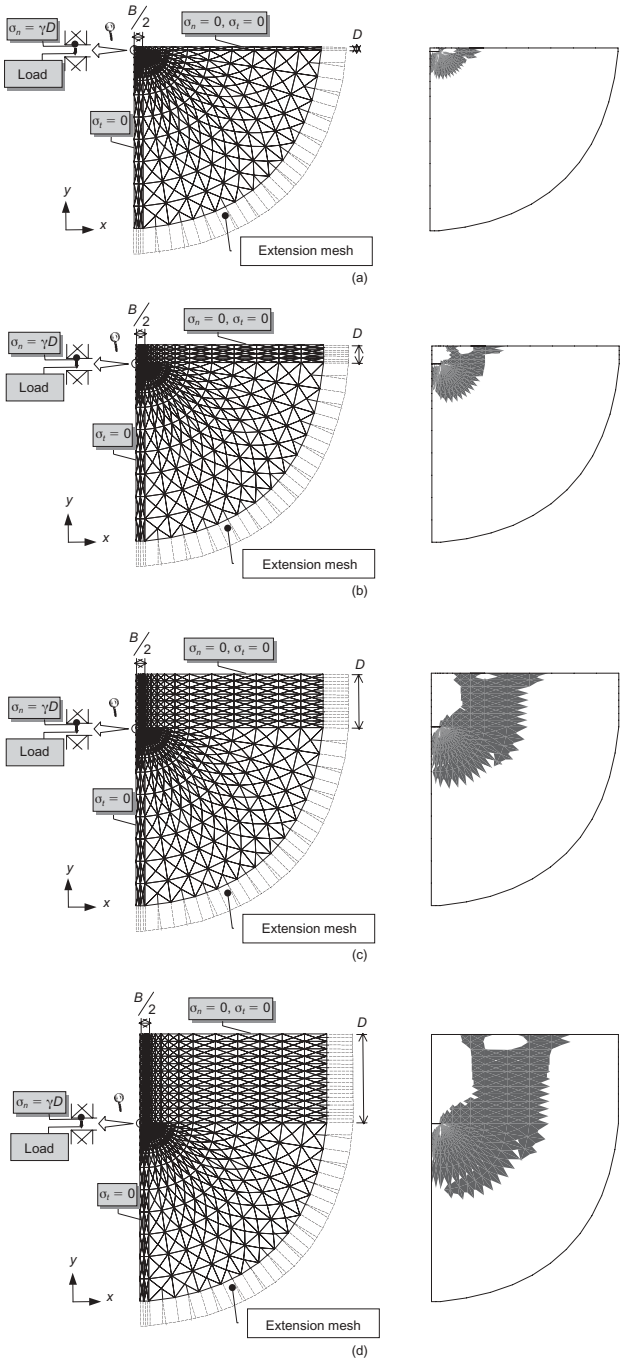

Fig. 6. Lower bound mesh and plasticity zones for strip footing with: (a) $D/B = 0{\cdot}2$; (b) $D/B = 1{\cdot}0$; (c) $D/B = 3{\cdot}0$; (d) $D/B = 5{\cdot}0$

capacity of embedded strip foundations is represented exactly by equation (1) with $s_c = 1$.

Figure 6 shows the lower bound stress fields, and Fig. 7 shows the upper bound velocity fields for both a surface and a deep foundation. It is clear from the figures that deeper foundations mobilise larger volumes of soil, dissipate more plastic energy, and show mechanisms where stress rotation becomes less important than for shallow foundations, with a considerable portion of the mechanism consisting of vertical slippage of the soil parallel to the sides of the foundation. These effects all require that more work be done by the applied load: hence the larger bearing capacities at larger D/B ratios.

The results of the lower and upper bound analysis of strip foundations bearing in clay are given in the second and third columns of Table 2. The lower and upper bounds on q_{bL}^{net} are very close, with maximum and minimum relative differences of 2·1% and 1·4% respectively. The agreement between upper and lower bounds on q_{bL}^{net} to this degree means that the q_{bL}^{net} values of Table 2 are exact for practical purposes.

For calculation of depth factors, we take the average of lower and upper bounds as the value of q_{bL}^{net}, as it provides a more systematic way of analysing the results. Since the exact value of N_c (5·14) is known for surface strip footings, it could be argued that the lower bound ($N_c = 5{\cdot}13$) is slightly better than the upper bound (5·20). The error in taking the average value of N_c at the surface is less than 0·5% and smaller than 1% for all the D/B values investigated. Depth factors are calculated by dividing the average of the lower and upper bound q_{bL}^{net} values at the various D/B values by q_{bL}^{net} for the surface foundation. They are plotted in Fig. 8 as a function of D/B. Fig. 8 also shows the plots of the Meyerhof (1951) and Brinch Hansen (1970) relationships for the depth factor, which are often used in practice, as well as of the simple relationship

$$d_c = 1 + 0{\cdot}27\sqrt{\frac{D}{B}} \tag{12}$$

which reproduces satisfactorily the relationship between d_c and D/B developed using the results of Table 2.

It can be seen from Fig. 8 that Meyerhof's depth factors are generally conservative within the range of depths ($D/B = 0$ to 2·5) for which they were defined, underpredicting the exact depth factors by as much as 9% for $0 < D/B < 2$ and overpredicting them slightly for $2 < D/B < 2{\cdot}5$. The Brinch Hansen factor was found to be adequate for $D/B < 0{\cdot}5$, but unconservative for higher values of D/B.

Circular, square and rectangular foundations shape factor

Values of q_{bL} for circular, square and rectangular footings (with $B/L = 2$, 3, 4 and 5) are given in Table 2. Referring to the values for circular footings on the surface, it is clear that the difference between lower and upper bound values is still small (6%), but is excessive (22%) for $D/B = 5$. Taking the average q_{bL}^{net} for $D/B = 5$ could therefore lead to errors of as much as 12·5%. This is the maximum error observed for any of our calculations; as B/L decreases from 1 to 0·2 for rectangular foundations, the relative difference between lower and upper bounds drops to roughly 12%, regardless of the value of D/B. We do our calculations both based on lower bound and average values of q_{bL}^{net}, but choose to recommend lower bound values for q_{bL}^{net} for use in design, as these are conservative.

If we directly divide the q_{bL}^{net} of circular, square and rectangular footings by the q_{bL}^{net} of the strip footing at the same D/B value, we obtain shape factor values that are not constant with depth. This is in contrast to the assumption of independence of shape and depth factors implied by traditional expressions. In order to derive consistent shape and depth factors, we take the depth factor at any given value of D/B to be expressed by equation (12) and compute the shape factor for the same D/B value by dividing the q_{bL}^{net} values from limit analysis for the circular, square and rectangular footings by the product of the q_{bL}^{net} of the strip footing by the depth factor expressed by equation (12). Mathematically:

$$s_c = \frac{q_{bL}^{net}}{d_c \left[q_{bL}^{net}\right]_{strip}} \tag{13}$$

The shape factors calculated from the average of the lower and upper bound values using equation (13) are plotted in Fig. 9 for footings of various shapes as a function of depth for D/B ranging from 0 to 4. They vary approximately with

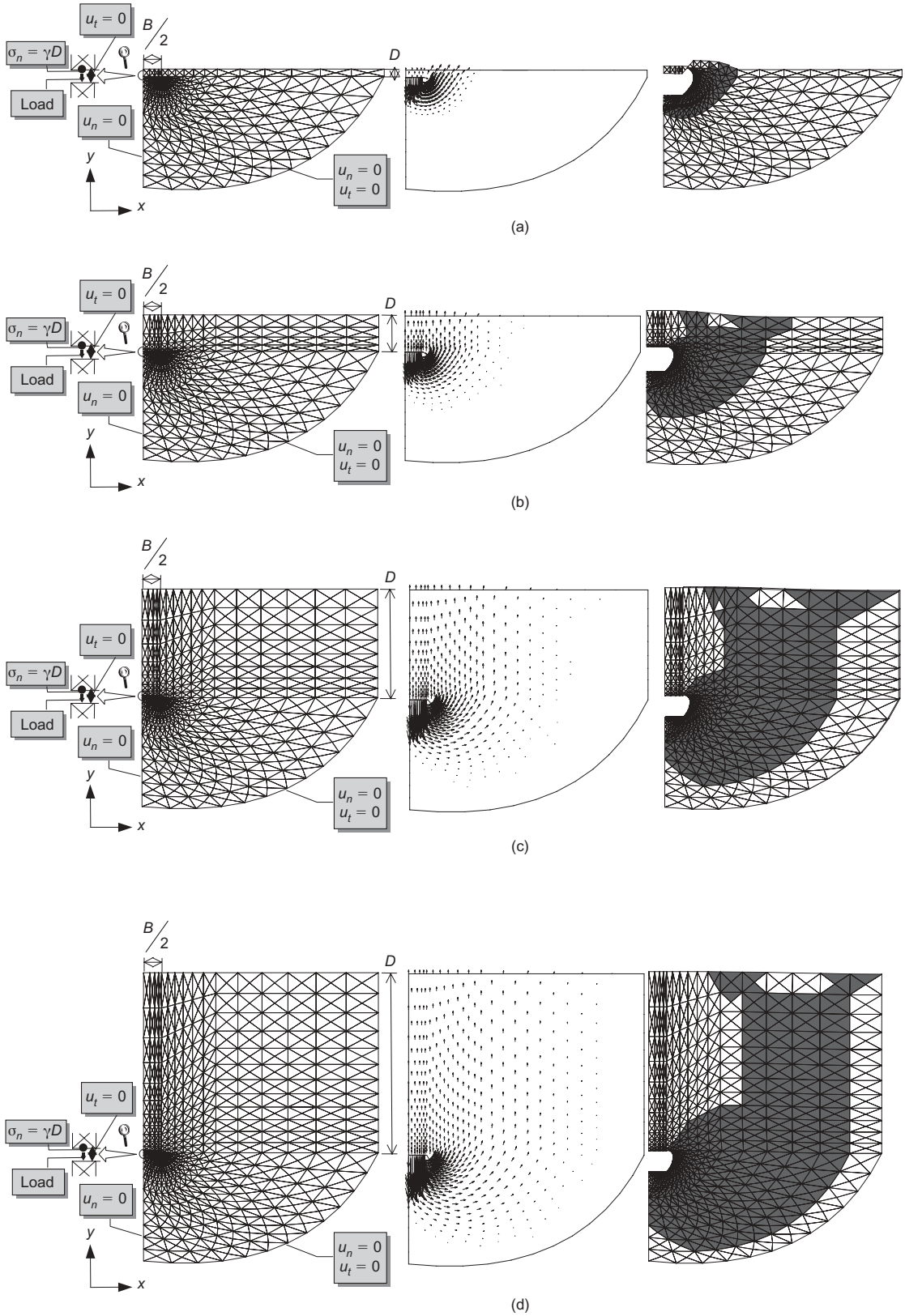

Fig. 7. Upper bound mesh and deformation pattern for strip footing with: (a) *D/B* = 0·2; (b) *D/B* = 1·0; (c) *D/B* = 3·0; (d) *D/B* = 5·0

the square root of D/B. The average value at the surface clearly drops towards 1 with decreasing B/L. Best-fit lines with the form

$$s_c = 1 + C_1 \frac{B}{L} + C_2 \sqrt{\frac{D}{B}} \tag{14}$$

are also plotted in Fig. 9. Note that the fit is excellent. Table 3 provides the values of C_1 and C_2 as a function of B/L.

It is apparent that the calculated shape factors for square and circular foundations are already deviating from trend at $D/B = 4$, the limit of the chart. Owing to the large difference between lower and upper bounds for $B/L = 1$ and

Table 2. Ratio of net bearing capacity factor to undrained shear strength, q_{bL}^{net}/s_u, for foundations in clay (L = lower, U = upper bound)

D/B	Strip		Circular		Square		Rectangular with B/L =							
							0·50		0·33		0·25		0·20	
	L	U	L	U	L	U	L	U	L	U	L	U	L	U
0·00	5·132	5·203	5·856	6·227	5·523	6·221	5·359	6·022	5·256	5·886	5·201	5·820	5·169	5·776
0·01	5·164	5·259	5·962	6·503	5·610	6·442	5·424	6·249	5·311	6·085	5·253	6·006	5·218	5·949
0·05	5·293	5·384	6·295	6·840	5·886	6·815	5·640	6·503	5·503	6·3003	5·430	6·203	5·389	6·126
0·10	5·448	5·548	6·491	7·140	6·171	7·130	5·860	6·756	5·697	6·533	5·614	6·413	5·565	6·321
0·20	5·696	5·806	6·897	7·523	6·590	7·524	6·197	7·116	5·997	6·867	5·895	6·731	5·836	6·637
0·40	6·029	6·133	7·303	8·104	7·194	8·096	6·680	7·574	6·408	7·271	6·272	7·113	6·190	7·003
0·60	6·240	6·341	7·866	8·608	7·671	8·573	7·082	7·993	6·740	7·608	6·567	7·412	6·465	7·299
0·80	6·411	6·509	8·370	9·034	8·068	8·996	7·427	8·377	7·030	7·936	6·817	7·705	6·695	7·570
1·00	6·562	6·657	8·771	9·429	8·429	9·346	7·729	8·724	7·297	8·240	7·048	7·976	6·904	7·819
2·00	7·130	7·227	9·973	11·008	9·752	10·853	8·968	10·055	8·447	9·476	8·109	9·086	7·860	8·835
3·00	7·547	7·652	10·686	12·140	10·532	12·000	9·860	11·076	9·296	10·473	8·920	10·026	8·607	9·696
4·00	7·885	7·994	10·954	13·030	10·941	12·900	10·513	11·878	10·018	11·242	9·594	10·769	9·249	10·403
5·00	8·168	8·284	10·998	13·743	11·206	13·640	10·880	12·545	10·464	11·887	10·117	11·408	9·796	11·030

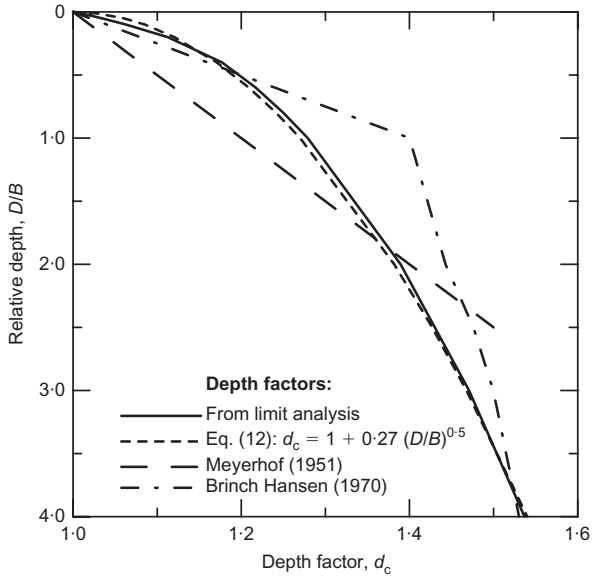

Fig. 8. Depth factors as calculated by finite element limit analysis, the proposed expression, and the expressions proposed by Meyerhof (1951) and Brinch Hansen (1970)

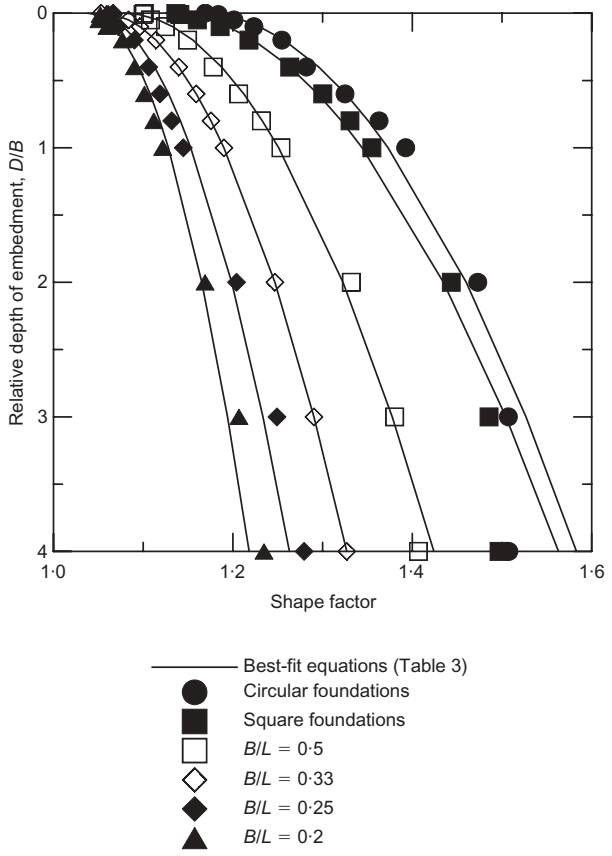

Fig. 9. Shape factor for foundations of various shapes as a function of relative depth as calculated by limit analysis plotted together with best-fit lines with the form of equation (14)

the deviation from trend for $D/B > 4$, results for $D/B > 4$ were not plotted in the figure.

The focus of the paper is on shallow foundations, defined traditionally as foundations for which $D/B \leqslant 1$ and usually with values of D/B at the low end of this range. A line that fits best all the data over $1 \leqslant L/B \leqslant 5$ and $0 \leqslant D/B \leqslant 1$ was obtained as

$$s_c = 1 + 0{\cdot}12\frac{B}{L} + 0{\cdot}17\sqrt{\frac{D}{B}} \tag{15}$$

This line is still quite accurate, deviating from the best-fit lines of Table 3 by no more than ±6% for $D/B \leqslant 1$. So it can be used in practice without significant loss of accuracy; this use is also more natural, as the constant C_1 does not depend on B/L, as it did for equation (14). The shape factor proposed by Meyerhof (1951) is plotted in Fig. 10 for square footings and rectangular footings with $B/L = 0{\cdot}2$. It is apparent that the Meyerhof (1951) shape factor is accurate only for footings placed directly on the surface of the deposit, significantly underpredicting the effect of B/L on the limit bearing capacity of deeper footings. The underprediction is quite significant, particularly when combined with the underprediction observed also for the depth factor, suggesting that designs based on the Meyerhof (1951) equation are overly conservative.

Deep foundations

Also of interest is the ratio q_{bL}^{net}/s_u of net bearing capacity to undrained shear strength for deep foundations (Fig. 11). This value has traditionally been taken as 9, but our results

Table 3. Regression constants in equation for the shape factor

B/L	C_1	C_2
1 (circle)	0·163	0·210
1 (square)	0·125	0·219
0·50	0·156	0·173
0·33	0·159	0·137
0·25	0·172	0·110
0·20	0·190	0·090

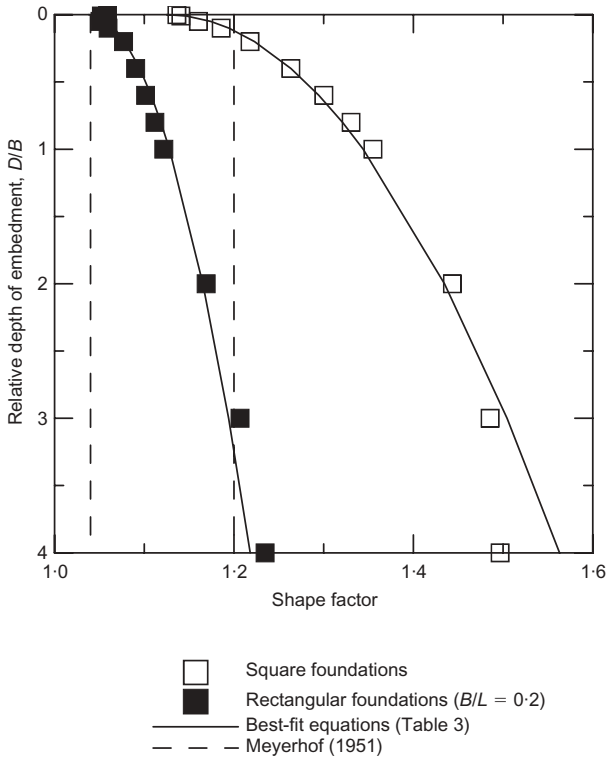

Fig. 10. Shape factors for square and rectangular footings with $B/L = 0{\cdot}2$ according to the limit analysis results, the best-fit equation (14), and the Meyerhof (1951) equation

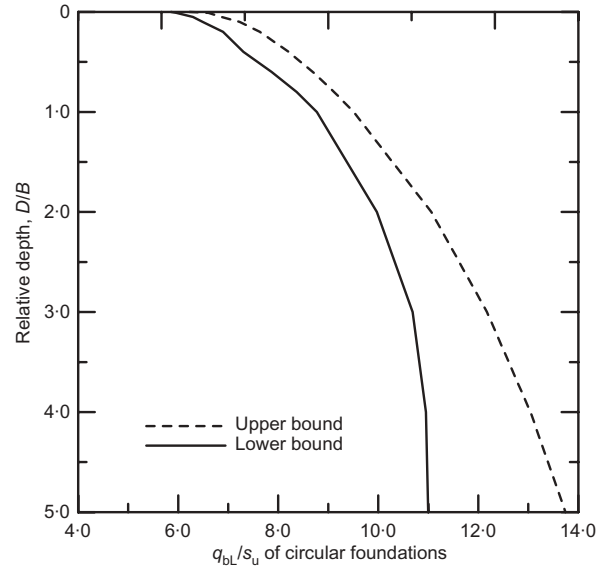

Fig. 11. Limit unit base resistance of circular foundations against depth

indicate that $q_{bL}^{net}/s_u > 9$ for $D/B > 1$. For $D/B = 5$ it is at least equal to 11, the value of the lower bound, and possibly as high as 13·7. It is possible that q_{bL}^{net}/s_u would continue to increase with increasing D/B beyond $D/B = 5$, as the flattening of the curve from $D/B = 4$ to $D/B = 5$ may be due to a mesh that is not sufficiently fine for such deep elements. These results suggest that the current practice in pile base capacity estimation may be as much as 20–30% over-conservative. However, it should be stressed that limit analysis may miss aspects of the interaction between foundation base and soil for deep foundations, which seems to be well approximated by a cavity expansion process. The assumptions made regarding the material in this paper (perfect plasticity and associated flow) may also have a more significant impact on the calculation of the end bearing of a deep foundation, which develops under more constrained conditions than that of a shallow foundation.

SUMMARY AND CONCLUSIONS

Limit analysis is a powerful technique for solving stability problems. In this paper, the lower and upper bounds of limit analysis are calculated for shallow foundation elements placed in clay. Calculations were done for rough strip, circular, square and rectangular foundations. Stress fields (in the case of lower bounds) and velocity fields (in the case of upper bounds) were optimised using non-linear optimisation techniques.

The equation normally used in practice for the shape factor was found to be excessively conservative, except for extremely low D/B values, which are not used in practice. Likewise, the Meyerhof (1951) equation for the depth factor was found to be conservative. However, the equation of Brinch Hansen (1970) was found to be adequate for $D/B < 0{\cdot}5$ and unconservative for higher values of D/B. Finally, although the unit base resistance of piles in clay is taken as $9s_u$ in practice, our calculations show that this may be 20–30% too conservative. Alternative, more accurate equations for both shape and depth factors are proposed.

Although it is not often realised, the safety factor that is used in current design practice accounts for various sources of uncertainty. These include analysis uncertainty, soil parameter uncertainty, construction uncertainties and load uncertainties. The results presented here reduce the uncertainties with respect to the bearing capacity equation, which can lead to lower factors of safety.

REFERENCES

Brinch Hansen, J. (1970). *A revised and extended formula for bearing capacity*, Bulletin No. 28. Danish Geotechnical Institute.

Davis, E. H. & Booker, J. R. (1973). The effect of increasing strength with depth on the bearing capacity of clays. *Géotechnique* **23**, No. 4, 551–563.

Drucker, D. C., Greenberg, W. & Prager, W. (1951). The safety factor of an elastic-plastic body in plane strain. *Trans. ASME, J. Appl. Mech.* **73**, 371.

Drucker, D. C., Prager, W. & Greenberg, H. J. (1952). Extended limit design theorems for continuous media. *Q. Appl. Math.* **9**, 381–389.

Eason, G. & Shield, R. T. (1960). The plastic indentation of a semi-infinite solid by a perfectly rough circular punch. *J. Appl. Math. Phys. (ZAMP)* **11**, 33–43.

Hill, R. (1951). On the state of stress in a plastic-rigid body at the yield point. *Phil. Mag.* **42**, 868–875.

Ladd, C. C., Foott, R., Ishihara, K., Schlosser, F. & Poulos, H.G. (1977). Stress-deformation and strength characteristics. *Proc. 9th Int. Conf. Soil Mech. Found. Engng, Tokyo* **2**, 421–494.

Lyamin, A. V. (1999). *Three-dimensional lower bound limit analysis using nonlinear programming*. PhD thesis, Department of Civil,

Surveying and Environmental Engineering, University of Newcastle, NSW.

Lyamin, A. V. & Sloan, S. W. (2002). Lower bound limit analysis using nonlinear programming. *Int. J. Numer. Methods Engng* **55**, 573–611.

Meyerhof, G. G. (1951). The ultimate bearing capacity of foundations. *Géotechnique* **2**, No. 4, 301–332.

Meyerhof, G. G. (1963). Some recent research on bearing capacity of foundations. *Can. Geotech. J.* **1**, 16–26.

Prandtl, L. (1920). Über die Härte Plasticher Körper. *Nachr. Ges. Wiss. Gött., Math-Phys. Kl.* **12**, 74–85.

Prandtl, L. (1921). Eindringungsfestigkeit und Festigkeit von Schneiden. *Zeit Angew. Math. Mech*. **1**, 15.

Skempton, A. W. (1951). The bearing capacity of clays. *Proceedings of the Building Research Congress*, Vol. 1, pp. 180–189.

Terzaghi, K. (1943). *Theoretical soil mechanics*. New York: Wiley.